CHAPTER- 5

Design of a low voltage TCNQ-Pd-Co@NC modified electrode-based NADH sensor

5.1 Introduction

The dihydro-nicotinamide adenine dinucleotide (NADH) is an essential coenzyme that participates in metabolic activities in live cells of all organisms [1,2]. It appears in the oxidized NAD^+ and reduced NADH form utilized during ATP formation. It serves as a hydrogen donor or electron transporter during photosynthesis, cellular redox respiration, and other processes [3,4]. There are over 300 NADH-dependent dehydrogenases for the maintenance of cellular metabolism, differentiation, energy metabolism, and various health disorders [5–7]. For example, NADH has a major control function in persons with Parkinson's disease, Alzheimer's disease, and depression [8–10]. Elevated NADH is associated with weariness, anxiety, and insomnia, all due to excessive NADH-dependent ATP generation [11]. Therefore, prospective chemical approaches for the determination of NADH have gained enormous attention. This suggested the development of NADH electrochemical sensors for NADH-dependent dehydrogenase. A significant overpotential may result in the direct electrochemical oxidation of NADH at a bare electrode. This, in turn, causes interferences from readily oxidizable compounds present in the actual samples. Recently, efforts have been made to develop electrochemical sensors by changing the electrode surface with suitable materials that efficiently overcome the kinetic barriers for the electrochemical resurgence of NAD^+ and increase electron transmission to reduce the large overpotentials [12,13]. Such sensors may be useful in multi-disciplines, including clinical biology, pollution monitoring, the food industry, and various bioprocess monitoring. In humans, NADH has been associated with mental health issues, diabetes, oxidative stress, cancer, neurological disorders, and reduced breathing capacity [14]. Moreover, the rate of NADH turnover in cancerous cells

is higher than in normal cells, indicating the potential use of NADH as a diagnostic tool in evaluating new cancer treatments [15]. Significantly, NADH may be consumed in the form of supplements, meals, or commodities like meat, fish, potatoes, avocados, etc. [16]. NADH concentration determination can help to evaluate the effect of certain drugs used in different diseases namely breast cancer [17]. For that reason, needed to construct a reliable and selective sensor for detecting NADH levels in food, environmental, and biological samples.

7,7,8,8-tetracyanoquinodimethane (TCNQ) is one of the most potent organic electron acceptors reported for the synthesis of semiconducting organic/inorganic charge-transfer compounds [18]. TCNQ forms a perfect electrode material for electrochemical biosensors due to its superior conductivity and electrocatalytic activity. TCNQ's advantageous electrical properties allow the efficient promotion of electron transport during the electrochemical reaction, enhancement of the sensitivity as well as the response signal of biosensors, and the reduction of response time. Additionally, owing to its enormous specific surface area, TCNQ can effectively increase active elements' loading, which enhances the sensor's sensitivity [19]. Its reduced forms ($TCNQ^{\bullet-}$ and $TCNQ^{2-}$) are the most suitable ligands for the production of a wide variety of metal-organic frameworks (MOFs) [20] and coordination polymers (CPs) [21] due to interaction with transition metal (TM) or organic cations. Although the development of sufficiently large, high-quality single crystals is appropriate for X-ray structural characterization, these materials are typically only sporadically soluble in organic solvents. These TCNQ-based materials have recently strained attention because of their strong magnetic characteristics and improved electrical conductivity. Since metals and their oxides have

strong conductivity and catalytic performance, they can boost the electron transfer efficiency and speed up the electrochemical reaction rate of TCNQ-based modified electrodes. Employing chemical reduction, physical adsorption, and electrochemical deposition, several metals and their oxides, including sodium, potassium [22], lithium, copper [23–25], silver [26], platinum, palladium [27], Fe_3O_4, CoO_3 [28], and ZnO [29] nanoparticles are loaded on the TCNQ surface.

Inorganic nanomaterials have become an intriguing research topic recently. Due to its remarkable catalytic capabilities, metal oxide-based modified electrodes have recently been found to have a high potential for the electrochemical assessment of numerous clinical indicators. Since the chemical and physical characteristics of nanomaterials differ from bulk materials, multiple approaches have been reported for the design of inorganic nanoparticles, including sol-gel [30], co-precipitation [31], and hydrothermal method [32]. The hydrothermal approach is an appealing method for the design of thermodynamically stable nanomaterial. Typically, sodium dodecyl sulfate, EDTA, and polyethyleneglycol have been used as a framework in hydrothermal methods [33]. The present work involves the design and validation of an electrochemical sensor for precise and selective sensing of nicotinamide adenine dinucleotide (NADH). The designed electrochemical sensor consists of TCNQ and Pd-Co@NC nanocomposite-modified electrodes (TCNQ-Pd-Co@NC/CPE). Pd-Co@NC and TCNQ offer excellent conductivity and good electrocatalytic performance for the electrochemical catalysis of NADH, including significantly reduced overpotential, high peak current, and good sensitivity. The designed electrode was validated by cyclic voltammetry, amperometry, and electrochemical impedance spectroscopy (EIS).

5.2 Experimental

5.2.1 Chemicals and apparatus

Tetracyanoquinodimethane, graphite powder (particle size < 20 μm), potassium tetrachloropalladate (II) [K_2PdCl_4], and Nujol oil (density 0.838 g/mL) were acquired from Sigma Aldrich Chemical Co., India. formaldehyde, cobalt chloride hexahydrate ($CoCl_2.6H_2O$), ethylene glycol, and potassium hydroxide were purchased from Merck, India. NADH, nitrilotriacetic acid (NTA), disodium hydrogen phosphate, dihydrogen sodium phosphate monohydrate, and melting point capillaries were procured from Sisco Research Laboratories (SRL) Pvt. Ltd. Isopropanol was received from SD Fine Chem Limited, India.

CHI 660E Inc., Texas, USA, was used for electrochemical experiments using a 2 mL cell with a three-electrode system. An electrode made of silver and silver chloride (RE 1B ALS Co. Ltd, Japan) was used as the reference, while a platinum (Pt) electrode was used as a counter electrode. The working electrode was modified TCNQ-Pd-Co@NC/CPE-based electrode. The buffer solution used was pH 7.0 phosphate buffer adjusted by HCL or NaOH using a digital pH meter (IKON).

5.2.2 Synthesis of PdNPs

PdNPs were synthesized by a modified method employed in our previous work [34]. Briefly, 100 μL ethylene glycol containing K_2PdCl_4 (20 mM) was mixed with 5 μL 3-APTMS (10 mM) in a cyclo mixture, further stirred to mix the two, followed by the addition of formaldehyde and microwave for about one minute. The mixture was

centrifuged to obtain a black color suspension washed in triplicate with water and then parched at 80 ^{0}C in a vacuum oven.

5.2.3 Synthesis of Co@NC

For the synthesis of Co-NTA, a previously reported hydrothermal method was used with slight modifications [35]. In brief, 0.1 mM cobalt chloride hexahydrate was dissolved in 15 ml of DI water in a 30 ml vial and ultrasonicated for 15 minutes. In another vial, 0.005 mol NTA was solvated in 15 ml of isopropyl alcohol and ultrasonicated for 15 minutes. The NTA solution was added to the cobalt chloride hexahydrate solution by drop-by-drop method followed by ultrasonication for 15 minutes. Then, the mixture of cobalt chloride hexahydrate and NTA solution was transferred to a 50 ml Teflon autoclave and warmed at 180 °C for about 6 h. The autoclave was cooled down to room temperature, which resulted in a pink color Co-NTA precipitate obtained at the bottom of the autoclave. The obtained precipitate was washed 5-6 times with DI water followed by ethanol washing, then centrifuged and parched at 60 ℃ for 10 h in a vacuum oven. The resultant Co-NTA powder was calcined at 600 ℃ in the furnace for 6 h to form cobalt nanocarbon (Co@NC).

5.2.4 Synthesis of Pd-Co@NC

For the synthesis of Pd-Co@NC, Co@NC suspension was first prepared by suspending 15 mg of Co@NC in 15 ml of double distilled water and bath sonication for 30 minutes. Then, 3 ml of PdNPs was added to Co@NC and bath sonicated for 30 minutes. The resultant Co@NC and PdNPs mixture was stirred on a magnetic stirrer at room temperature overnight. Thereafter, the resultant system was centrifuged at 12000 rpm for

collecting Pd-Co@NC, followed by washing with double distilled water and ethanol in triplicate. The supernatant was discarded, and the residue obtained was dried for 10 hours in a vacuum oven at 60 °C.

5.2.5 Fabrication of TCNQ-Pd-Co@NC modified carbon paste electrodes

The synthesized Pd-Co@NC was geometrically mixed with graphite powder. Then, TCNQ and a few drops of Nujol oil were mixed thoroughly to form a homogenous paste. Nujol oil was used as a binder to avoid leaching from modified carbon paste during electroanalysis. The electrode body was filled with the modified electrode paste (Table 5.1), and a copper wire was connected to the electrodes. The modified carbon paste electrode surface was smoothed on clean butter paper.

Table 5.1 Composition of the modified carbon paste electrodes.

System	TCNQ (w/w) %	Co@NC (w/w) %	Pd-Co@NC (w/w) %	Graphite (w/w) %	Nujol oil (w/w) %
TCNQ/CPE	4	-	-	71	25
TCNQ-Co@NC/CPE	4	10	-	61	25
TCNQ-Pd-Co@NC/CPE	4	-	10	61	25

5.2.6 Electrochemical measurements

Electrochemical measurement was accomplished using a three-electrode system equipped with 2 ml 0.1 M PBS (pH 7.0) on an Electrochemical Workstation Model No CHI (660E), Inc. Austin, TX, USA. The three electrodes used were Ag/AgCl, Platinum wire, and TCNQ-PdCo@NC/CPE modified electrode as reference, counter/supporting, and working electrode, respectively. During electrochemical measurement, cyclic voltammetry, amperometry, and electrochemical impedance spectroscopy (EIS) were

done against various concentrations of NADH. The electrode was checked to determine the effect of pH, Interference, stability, and reproducibility of TCNQ-Pd-Co@NC. The electrode was also studied for real-time analysis of NADH spiked in avocado juice.

5.3 Results and Discussion

5.3.1 Characterization of Co@NC and Pd-Co@NC

The crystalline properties, structural assessment, and phase uniformity of Co@NC and Pd-Co@NC have been determined by powder X-ray diffraction technique. The XRD spectrum of Co@NC shows the diffraction peak of metallic cobalt at 2θ values 44.20°, 51.45°, and 75.85° correspond to planes (111), (200), and (220), respectively [36,37]. All the peaks were well-matched with the JCPDS file number 15-0806. A wide diffraction peak at 26.38° related to the (002) plane is due to the presence of graphitic carbon which is shown in Figure 5.1 (a). The Pd-Co@NC shows the characteristic peak of palladium metal at 40.16° and 47.43° corresponding to planes (111) and (200) which matched with the JCPDS file number 87-641 [34]. 2θ value at 26.72° shows (002) of graphitic carbon. Peaks at 44.35, 51.51, and 75.95 exhibited (111), (200), and (220) planes of metallic cobalt as shown in Figure 5.1 (b).

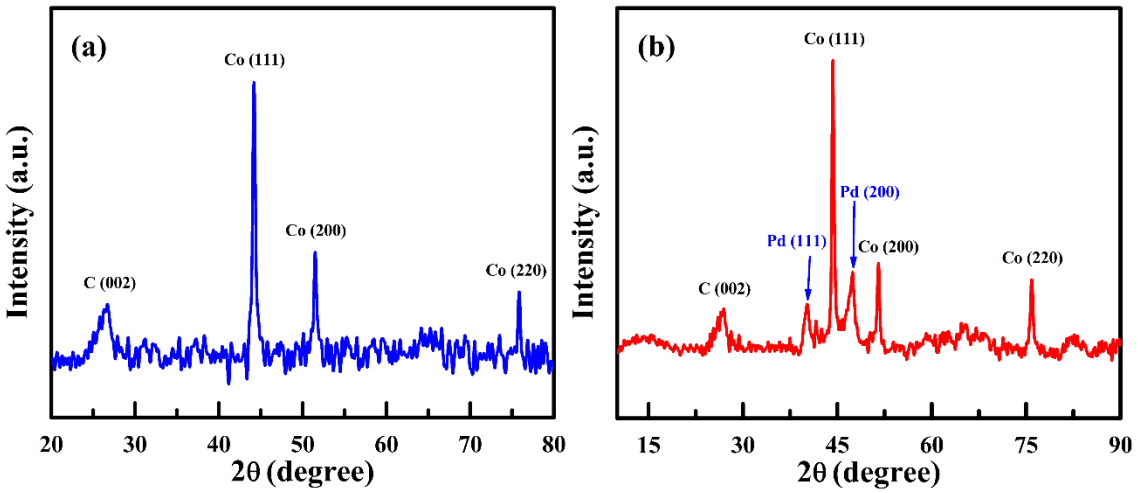

Figure 5.1 XRD Spectrum of (a) Co@NC and (b) Pd-Co@NC.

The XPS technique was used to analyze the chemical composition and metallic state of the as-synthesized Pd-Co@NC catalyst. Figure 5.2 (a) shows the XPS spectrum of the Pd 3d. The spectrum peaks are deconvoluted into four distinct peaks with binding energies of around 335.43 eV, 336.98 eV, 340.74 eV, and 342.40 eV, which correspond to $3d_{5/2}$ and $3d_{3/2}$. The two peaks, at 335.43 eV and 340.74 eV, show the metallic form of Pd, and the subsequent peaks, at 336.98 eV and 342.40 eV, exhibit the Pd (II) state [38]. The XPS spectrum of Co 2p is deconvoluted into two peaks along with the satellite peaks which are centered at 785.58 eV and 802.38 eV corresponding to the Co $2p_{3/2}$ and Co $2p_{1/2}$, respectively [39] as shown in Figure 5.2 (b). Figure 5.2 (c) demonstrates the C 1s spectrum of Pd-Co@NC in which the peaks at 284.57 eV, 285.7 eV, and 288.11 eV, correspond to C-C, C=N, and C-O bonds, respectively. The N 1s shows the binding energy at 399.86 eV, and 400.61 eV represents the C-N and C=N bonds, respectively [40] shown in Figure 5.2 (d).

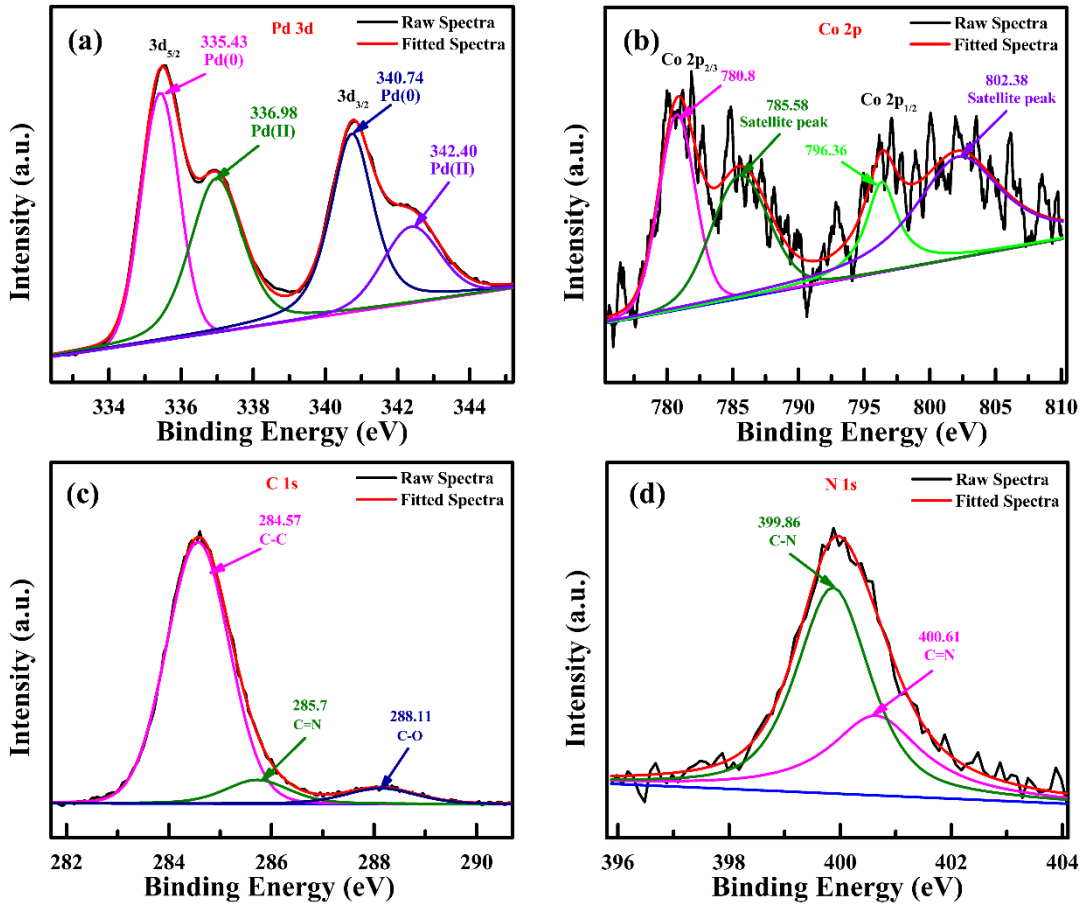

Figure 5.2 XPS spectra of Pd-Co@NC (a) Pd 3d, (b) Co 2p, (c) C 1s, and (d) N 1s.

Hydrothermally synthesized Co@NC was characterized for morphology using SEM. Co@NC were irregularly shaped (Figure 5.3 (a)), while Pd-Co@NC were spherical, and small particles of palladium were also present along with Co@NC as can be observed in Figure 5.3 (d). TEM analysis also revealed Co@NC as irregular-shaped particles of size 25 nm, while Pd-Co@NC were about 50 nm spherical particles as shown in Figure 5.3 (b) & (e). Pd-Co@NC was observed as aggregates of Pd and Co@NC, where Pd was observed as doped particles on the surface of Co@NC. The SAED pattern confirmed the crystalline nature of particles as exhibited in Figure 5.3 (c) & (f).

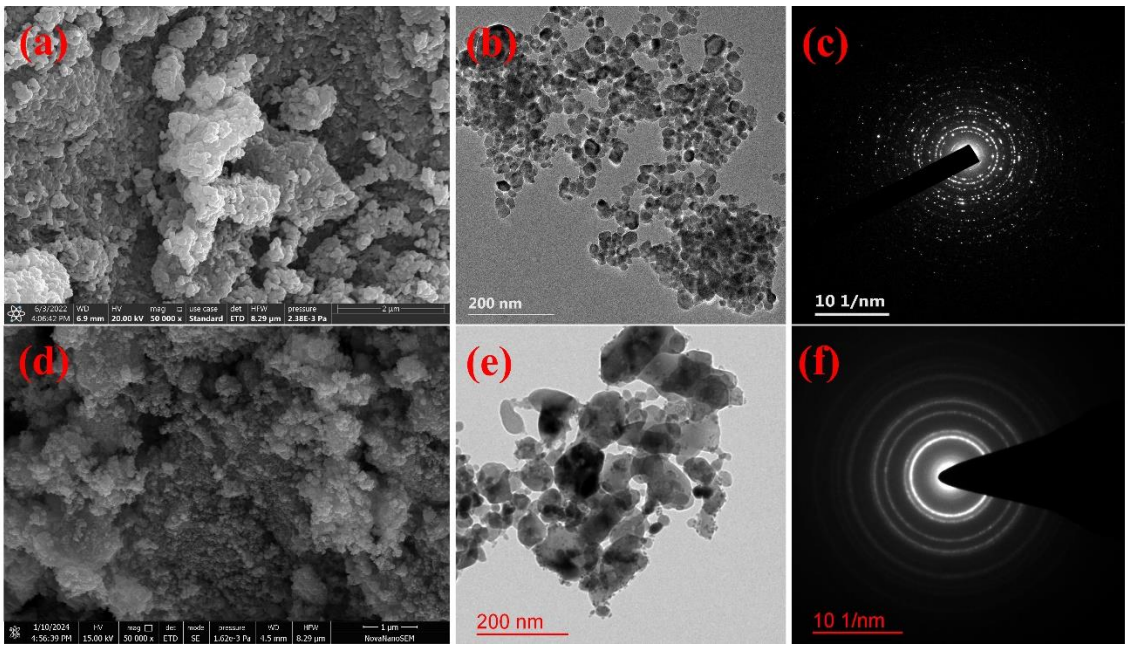

Figure 5.3 SEM, TEM, and SAED images of Co@NC (a, b, c) and Pd-Co@NC (d, e, f), respectively.

5.3.2 Cyclic voltammetry analysis

A cyclic voltammetry study was conducted to determine the NADH sensing potency of modified electrodes. Figure 5.4 illustrates the cyclic voltammogram for the oxidation of NADH on TCNQ/CPE, TCNQ-Co@NC/CPE, and TCNQ-Pd-Co@NC/CPE modified electrodes. The intensity of cathodic and anodic peak currents increases in the order of TCNQ/CPE, TCNQ-Co@NC/CPE, and TCNQ-Pd-Co@NC/CPE. The peak-to-peak separation value (ΔE_p) value was 210 mV for TCNQ/CPE, 202 mV for TCNQ-Co@NC/CPE, and 189 mV for TCNQ-Pd-Co@NC/CPE as shown in Figure 5.4 (a), (b), and (c), respectively. The results indicated that electron transfer at the electrode /electrolyte interface was fastened in the case of TCNQ-Pd-Co@NC/CPE than TCNQ-Co@NC/CPE and TCNQ/CPE, probably due to the better conductivity of TCNQ-Pd-Co@NC/CPE.

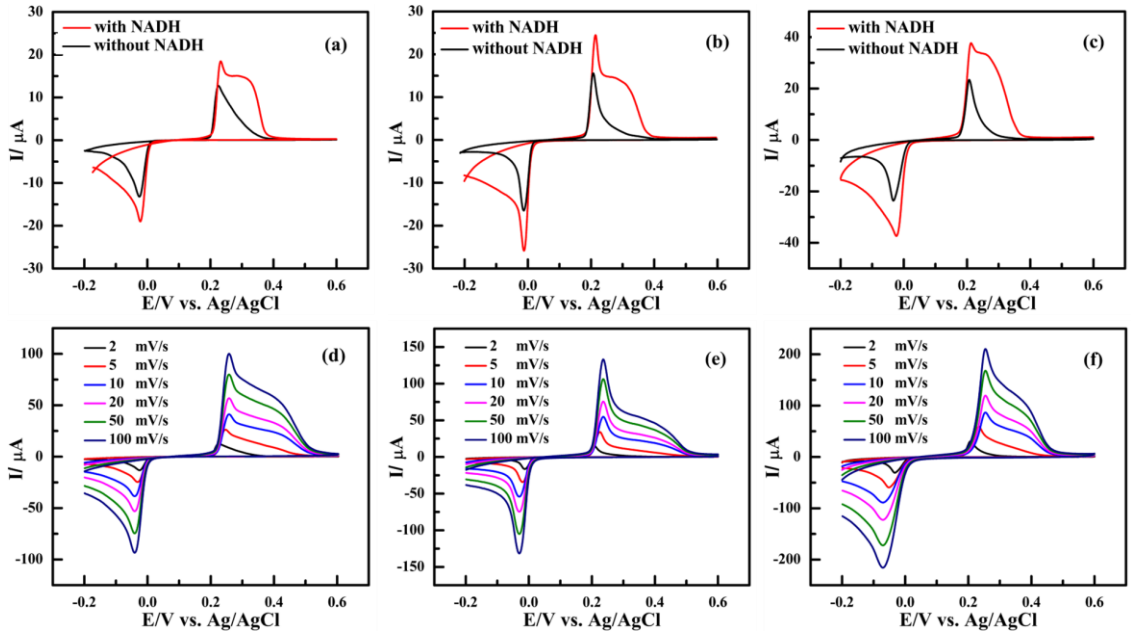

Figure 5.4 Cyclic voltammograms in the absence/presence of 50 µM NADH (a) TCNQ/CPE (b) TCNQ-Co@NC/CPE and (c) TCNQ-Pd-Co@NC/CPE at 2 mV/s scan rates; Cyclic voltammograms of (c) TCNQ/CPE (d) TCNQ-Co@NC/CPE and (e) TCNQ-Pd-Co@NC/CPE at 2 to 100 mV/s scan rate in the absence of NADH.

Changes in voltammetric scan rate also play a key role in the sensing potency of electrodes. The rise and fall in scan rate change the magnitude of peak current, which may have a significant effect on electrode output. For example, a rise in scan rate results in an increase in the magnitude of the peak current. Therefore, the effect of scan rate on the electrocatalytic performance of TCNQ/CPE, TCNQ-Co@NC/CPE, and TCNQ-Pd-Co@NC/CPE was investigated towards their NADH oxidation potential. The scan rate employed ranged from 2-100 mV/s for 50 µM of NADH in 0.1 M phosphate buffer (pH 7.0). The results of Figure 5.5 (a), (b), and (c) showed that increasing the scan rate raises the current response as a response of which higher current was observed. The current intensity was maximum with TCNQ-Pd-Co@NC/CPE while lowest in TCNQ/CPE. Herein, the anodic and cathodic current increased with the scan rate; however, the

difference in peak potential remained almost the same. Therefore, a linear relationship between the peak current and square root of the scan rate was observed, concluding a diffusion-controlled NADH oxidation at the modified electrode TCNQ-Pd-Co@NC/CPE [1,2].

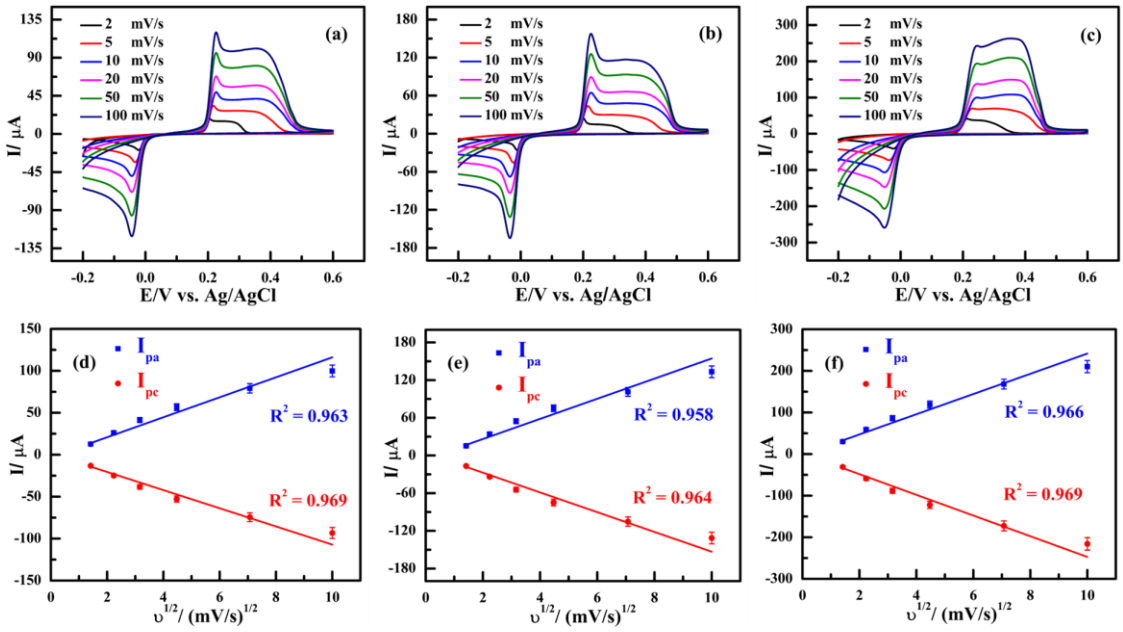

Figure 5.5 Cyclic voltammograms for (a) TCNQ/CPE, (b) TCNQ-Co@NC/CPE, and (c) TCNQ-Pd-Co@NC/CPE at different scan rates of 2 to 100 mV/s with 50 µM NADH; A plot of anodic/cathodic current versus square root of scan rate for (d) TCNQ/CPE, (e) TCNQ-Co@NC/CPE and (f) TCNQ-Pd-Co@NC/CPE.

The cyclic voltammograms observed above at different scan rates were plotted as peak current vs. square root of the scan rate in order to monitor the change in voltammetric response with the scan rate over time. As observed in Figures 5.5 (d), (e), & (f), a direct relationship between the peak current and the square root of the scan rate was observed. In addition, the Randles–Sevcik equation [41] was used to calculate the electrochemical active surface area (EASA) of TCNQ/CPE, TCNQ-Co@NC/CPE, and TCNQ-Pd-Co@NC/CPE using equation (5.1)

$$\mathbf{I_p = (2 \cdot 69 * 10^5) n^{3/2} A D^{1/2} \nu^{1/2} C_0} \quad (5.1)$$

Where I_p is the peak current (A), n is the number of electrons involved during the reaction, A is the electrochemically active surface area (cm^2), D is the diffusion coefficient of NADH (6.9 x 10^{-6} cm^2 s^{-1} at 25 °C), υ is the scan rate (V s^{-1}), and C_0 is the concentration of the electroactive analytes (mol cm^{-3}). Putting these values in equation (5.1), the EASA of TCNQ/CPE, TCNQ-Co@NC/CPE, and TCNQ-Pd-Co@NC/CPE calculated to be 0.0673 cm^2, 0.2586 cm^2, and 0.2950 cm^2, respectively. The EASA value demonstrated that TCNQ-Pd-Co@NC/CPE has superior electrochemical performance than TCNQ/CPE and TCNQ-Co@NC/CPE. Therefore, TCNQ-Pd-Co@NC/CPE provided an effective platform for the electrochemical oxidation of NADH. The study revealed the superior capability of TCNQ-Pd-Co@NC/CPE based electrode in charge transfer than TCNQ/CPE and TCNQ-Co@NC/CPE, validating better conductivity of TCNQ-Pd-Co@NC/CPE for NADH sensing.

5.3.3 Amperometric detection of NADH

Amperometric measurements under stirring conditions were done to evaluate the electroanalytical capabilities of the designed electrodes. The records were obtained at 0.2 V vs. Ag/AgCl potential with 10 µM to 250 µM NADH. TCNQ-Pd-Co@NC/CPE modified electrodes showed an instant response and reached steady-state within three seconds compared to TCNQ-Co@NC/CPE and TCNQ/CPE modified electrodes as shown in Figure 5.6 (a), (b), and (c). The standard curve prepared for NADH sensing by amperometry was observed as a linear relationship between current and NADH concentration Figure 5.6 (d). The electrode sensitivity observed for NADH sensing was

determined as slope and was 5.5, 11.3, and 21.5 µA/mM for TCNQ/CPE, TCNQ-Co@NC/CPE, and TCNQ-Pd-Co@NC/CPE electrodes, respectively. The lowest limit of detection was 5.17 µM in TCNQ-Pd-Co@NC/CPE, calculated using the equation (5.2) [42].

$$\mathbf{LOD} = \mathbf{3} * \mathbf{SD/m} \tag{5.2}$$

Where SD is the standard deviation in the intercept and m is the slope of the linearly fitted curve.

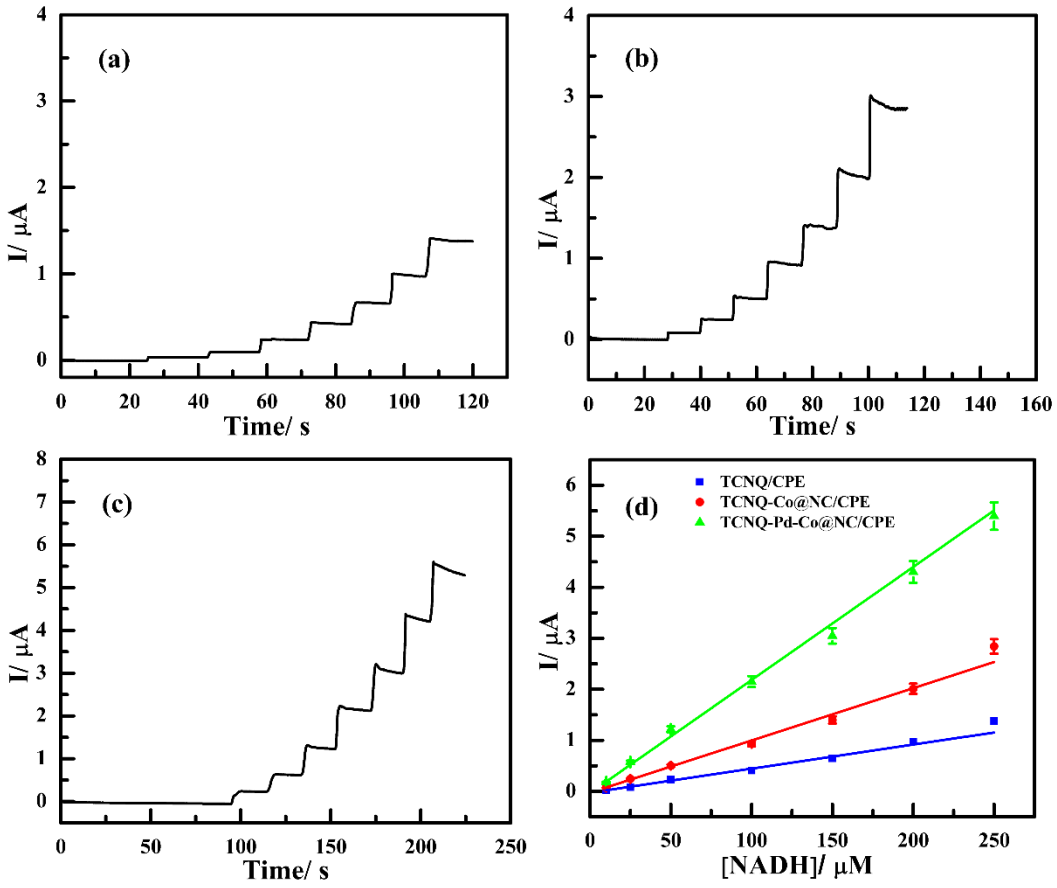

Figure 5.6 Amperometric responses of (a) TCNQ/CPE, (b) TCNQ-Co@NC/CPE & (c) TCNQ-Pd-Co@NC/CPE on the addition of varying concentrations of NADH from 10 µM to 250 µM recorded at a constant potential of 0.2 V vs. Ag/AgCl; (d) Calibration curve current versus NADH concentration.

5.3.4 Electrochemical impedance spectroscopy (EIS)

EIS has been widely used for investigating the characteristics of the electrode and determining the information about the transfer of electrons between the electrolyte and electrode surface. The EIS data was fitted on R(CR)W circuit by using ZSimpWin software. In EIS, the semi-circular portion at higher frequencies corresponds to the electron transfer, while the linear part at lower frequencies corresponds to the diffusion control process. The semicircle's diameter is equivalent to the electron transfer resistance (R_{ct}), demonstrating the extent of sensitivity of the modified layer [43]. The lower the R_{ct} value, the higher the electron transfer capability and thus sensitivity towards NADH. The Nyquist plots in the frequency range of 1 Hz to 1000 kHz for TCNQ/CPE, TCNQ-Co@NC/CPE, and TCNQ-Pd-Co@NC/CPE showed a straight line in the low-frequency domain, and a semicircle in the high-frequency environment as shown in Figure 5.7.

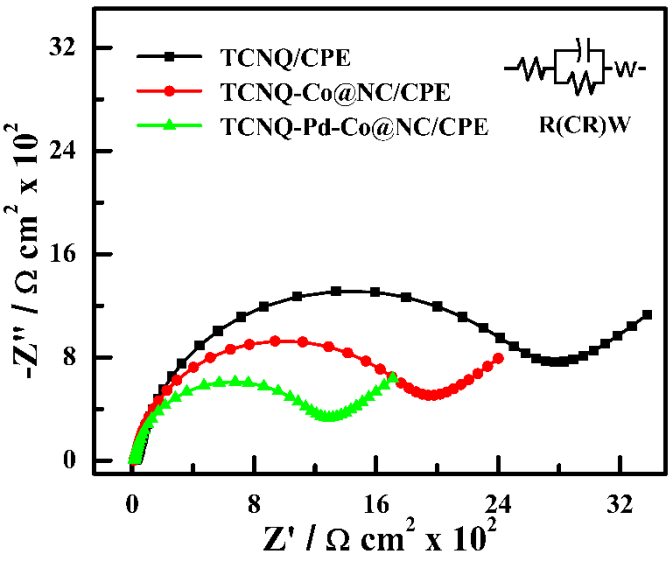

Figure 5.7 Nyquist plots in 0.1 M phosphate buffer solution (pH 7.0) over the frequency range 1 Hz to 1000 kHz in 50 µM NADH.

Nyquist plot is completely semicircle showing Warburg diffusion. Here Warburg impedance arises due to the diffusion control reaction of NADH during the electrochemical process. The redox reaction occurs at the electrode due to the diffusion of NADH in the solution toward the electrode surface [44]. At high frequencies, diffusion effects are minimal because the applied AC signal frequency is too fast for diffusion to respond. However, at lower frequencies, diffusion becomes more significant as the NADH takes time to reach the electrode surface. This gives rise to the Warburg element in the Nyquist plot, represented as a diagonal line with a slope of 45°, transitioning to a vertical line at even lower frequencies (Figure 5.7). The Warburg impedance can be expressed by [45,46] (Equation 5.3)

$$\boldsymbol{Zw = \sigma\left(\frac{1-j}{\sqrt{w}}\right)} \quad (5.3)$$

Where Zw is the Warburg impedance, σ is the Warburg coefficient, w is the angular frequency, and j is the imaginary unit.

The R_{ct} value for the three electrodes was in decreasing order of TCNQ/CPE (27.5 x 10^2 Ω cm^2), TCNQ-Co@NC/CPE (19.2 x 10^2 Ω cm^2), and TCNQ-Pd-Co@NC/CPE (12.5 x 10^2 Ω cm^2). From this R_{ct} value, it is clear that TCNQ-Pd-Co@NC/CPE shows higher electron transfer and lower diffusion control than TCNQ-Co@NC/CPE and TCNQ/CPE. The higher electron transfer in TCNQ-Pd-Co@NC/CPE is due to the synergistic interaction between Pd and Co. Thus, we can say that the incorporation of Pd significantly improved the electron transfer capability of Co@NC.

Table 5.2 Comparison of sensitivity, working potential, and detection limit of the designed TCNQ-Pd-Co@NC/CPE electrode with previously reported electrode value for NADH detection.

Working electrode	**E_p (V)**	**Sensitivity ($\mu A\ mM^{-1}$)**	**Limit of Detection (μM)**	**References**
TCNQ-Pd-Co@NC/CPE	+ 0.20	21.50	5.17	This work
TCNQ-Co@NC/CPE	+ 0.20	11.30	12.83	This work
TCNQ/CPE	+ 0.20	5.50	23.76	This work
PB-rGO/GCE	+ 0.50	10.00	63.50	[47]
Graphene/GCE	+ 0.50	12.60	20.00	[48]
Co_3O_4 nanoparticle/carbon ink	+ 0.25	14.00	0.53	[49]
Chemically reduced graphene oxide/GCE	+ 0.45	2.68	10.00	[50]
Poly-phenothiazine/GCE	+ 0.20	1.82	3.40	[51]

PB = Prussian blue, rGO = reduced Graphene oxide

5.3.5 Effect of pH on TCNQ-Pd-Co@NC/CPE, interference, stability, and reproducibility of TCNQ-Pd-Co@NC/CPE

The pH of the buffer solution also plays a major role in NADH detection. The effect of pH on NADH's electrochemical behavior was studied by cyclic voltammetry in 0.1 M phosphate buffers at different pH values (pH 5-9). The study showed that a maximum peak current at a pH of 7.0 was observed, and the peak current decreased when the pH

value was altered (Figure 5.8 (a)). Since selectivity is a prerequisite for all sensors, evaluating designed sensors in the presence of interferent molecules is a must. Herein, the interferent investigation for TCNQ-Pd-Co@NC/CPE-modified electrode was confirmed by amperometric analysis in the presence of 25 µM NADH. The result showed high sensitivity of the electrode toward NADH and had selective and precise detection capability even in the presence of other contending biomolecules like glucose, dopamine, and uric acid (Figure 5.8 (b)).

Electrochemical sensing efficiency, stability, and repeatability are other essential characteristics of electrodes. Therefore, the operational stability of TCNQ-Pd-Co@NC/CPE was determined by storing the manufactured sensor at room temperature for 5, 10, and 15 days and studying it against NADH. The oxidative peak current with 50 µM NADH does not change significantly, showing good efficiency and stability as shown in Figure 5.8 (c). The five-fold cyclic voltammetry result of the sensor for 50 µM NADH was almost constant. The standard deviation was 0.32 %, and the relative standard deviation was 1.44 %, as shown in Figure 5.8 (d). This indicated good reproducibility of the sensor for NADH.

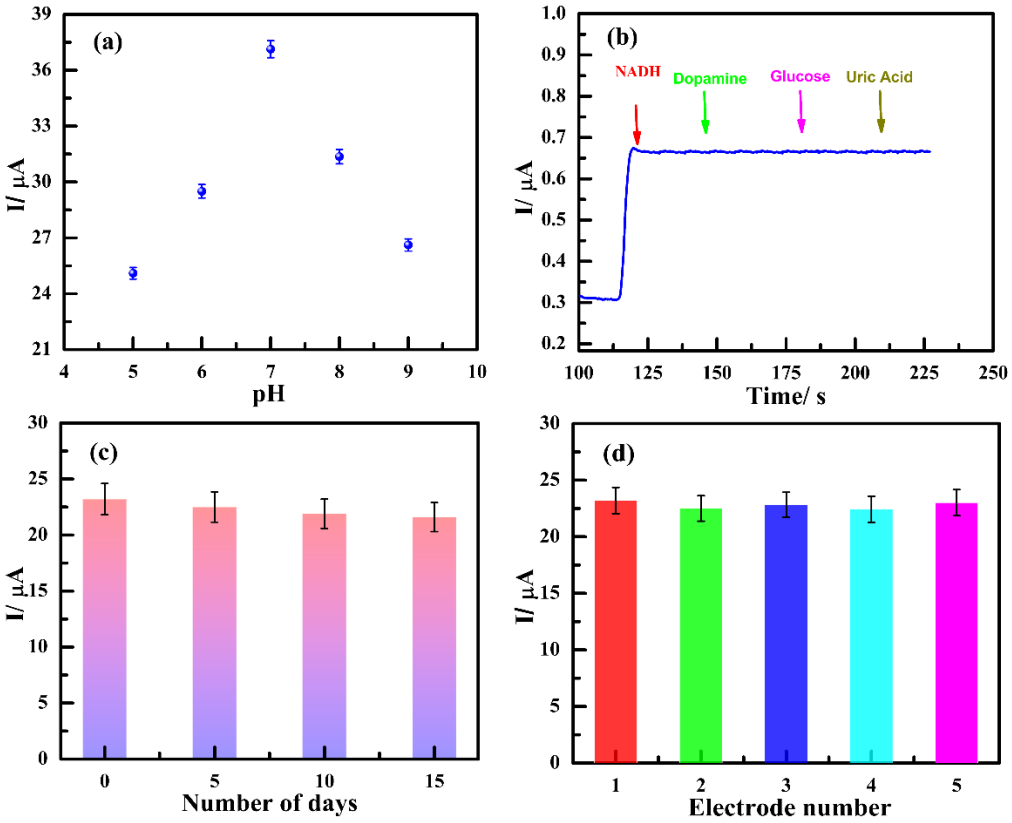

Figure 5.8 (a) Effect of pH on TCNQ-Pd-Co@NC/CPE (b) interference (c) stability, and (d) reproducibility of TCNQ-Pd-Co@NC/CPE.

5.3.6 Real sample analysis

Real sample analysis was performed in avocado juice using the standard addition method to determine the practical significance of the newly designed TCNQ-Pd-Co@NC/CPE sensor. Avocado juice samples were spiked with 10, 50, and 100 µM NADH in 0.1 M phosphate buffer, and amperometry was carried out at 0.20 V vs. Ag/AgCl. The recovered amounts ranged from 95.20 to 99.65 % (Table 5.3). The results showed that the modified electrode-based sensor is capable of identifying specific analytes in the collected sample for real sample analysis.

Table 5.3 Real sample analysis of NADH in avocado juice sample.

Sample No	Amount Used (µM)	Amount *Found (µM)	Recovery (%)
1	10	9.60 ± 0.14	95.20
2	50	49.15 ± 1.72	95.78
3	100	100.28 ± 0.73	99.65

* Repeated three times (n=3).

5.4 Conclusions

The present work involves the design of modified TCNQ-Pd-Co@NC nanocomposites-based carbon paste electrodes sensitive to NADH. Designed nanocomposite-modified electrodes demonstrated strong electrocatalytic performance for NADH oxidation at a relatively low potential. Cyclic voltammetry, amperometry, and electrochemical impedance spectroscopy methods determined the efficacy of the electrode. TCNQ-Pd-Co@NC modified carbon paste electrode demonstrated a high sensitivity of 21.50 µA mM^{-1} with a LOD of 5.17 µM. R_{ct} value of TCNQ-Pd-Co@NC/CPE was 12 x 10^2 Ω cm^2, confirming that the modified electrode exhibited better electrocatalytic behavior. Modified electrodes displayed excellent analytical efficiency, outstanding stability, and repeatability for NADH detection. Therefore, designed TCNQ-Pd-Co@NC nanocomposites-based carbon paste electrodes can be efficiently used for precise and selective NADH sensing.

5.5 References

[1] A.R. Marlinda, S. Sagadevan, N. Yusoff, A. Pandikumar, N.M. Huang, O. Akbarzadeh, M.R. Johan, Gold nanorods-coated reduced graphene oxide as a modified electrode for the electrochemical sensory detection of NADH, J Alloys Compd 847 (2020) 156552. https://doi.org/10.1016/j.jallcom.2020.156552.

[2] J. Li, Q. Sun, Y. Mao, Z. Bai, X. Ning, J. Zheng, Sensitive and low-potential detection of NADH based on boronic acid functionalized multi-walled carbon nanotubes coupling with an electrocatalysis, Journal of Electroanalytical Chemistry 794 (2017) 1–7. https://doi.org/10.1016/j.jelechem.2017.03.042.

[3] T. Rębiś, M. Kuznowicz, A. Jędrzak, G. Milczarek, T. Jesionowski, Design and fabrication of low potential NADH-sensor based on poly(caffeic acid)@multi-walled carbon nanotubes, Electrochim Acta 386 (2021) 138384. https://doi.org/10.1016/j.electacta.2021.138384.

[4] X. Huang, I.H. El-Sayed, X. Yi, M.A. El-Sayed, Gold nanoparticles: Catalyst for the oxidation of NADH to NAD+, J Photochem Photobiol B 81 (2005) 76–83. https://doi.org/10.1016/j.jphotobiol.2005.05.010.

[5] M. Eguílaz, F. Gutierrez, J.M. González-Domínguez, M.T. Martínez, G. Rivas, Single-walled carbon nanotubes covalently functionalized with polytyrosine: A new material for the development of NADH-based biosensors, Biosens Bioelectron 86 (2016) 308–314. https://doi.org/10.1016/j.bios.2016.06.003.

[6] C.H. Chen, Y.C. Chen, M.S. Lin, Amperometric determination of NADH with Co3O4 nanosheet modified electrode, Biosens Bioelectron 42 (2013) 379–384. https://doi.org/10.1016/j.bios.2012.10.086.

[7] L. Li, H. Lu, L. Deng, A sensitive NADH and ethanol biosensor based on graphene-Au nanorods nanocomposites, Talanta 113 (2013) 1–6. https://doi.org/10.1016/j.talanta.2013.03.074.

[8] S. Chen, K. Shang, X. Gao, X. Wang, The development of NAD+-dependent dehydrogenase screen-printed biosensor based on enzyme and nanoporous gold co-catalytic strategy, Biosens Bioelectron 211 (2022) 114376. https://doi.org/10.1016/j.bios.2022.114376.

[9] W.D. Cameron, C. V. Bui, A. Hutchinson, P. Loppnau, S. Gräslund, J. V. Rocheleau, Apollo-NADP+: A spectrally tunable family of genetically encoded

sensors for NADP+, Nat Methods 13 (2016) 352–358. https://doi.org/10.1038/nmeth.3764.

[10] J. Lu, Y. Liu, X. Liu, X. Lu, X. Liu, Construction of a highly sensitive NADH sensing platform based on PDDA-rGO nanocomposite modified electrode, Ionics (Kiel) 22 (2016) 2225–2233. https://doi.org/10.1007/s11581-016-1753-7.

[11] P. Manusha, S. Senthilkumar, Development of a ferrocene-tethered ionic liquid modified electrode for non-enzymatic electrochemical sensing of NADH, Journal of Materials Science: Materials in Electronics 33 (2022) 8576–8585. https://doi.org/10.1007/s10854-021-06576-0.

[12] B.K. Jena, C.R. Raj, Electrochemical biosensor based on integrated assembly of dehydrogenase enzymes and gold nanoparticles, Anal Chem 78 (2006) 6332–6339. https://doi.org/10.1021/ac052143f.

[13] F. Valentini, A. Salis, A. Curulli, G. Palleschi, Chemical reversibility and stable low-potential NADH detection with nonconventional conducting polymer nanotubule modified glassy carbon electrodes, Anal Chem 76 (2004) 3244–3248. https://doi.org/10.1021/ac034888w.

[14] Y. Liu, R. Landick, S. Raman, A Regulatory NADH/NAD+ Redox Biosensor for Bacteria, ACS Synth Biol 8 (2019) 264–273. https://doi.org/10.1021/acssynbio.8b00485.

[15] M. Labib, E.H. Sargent, S.O. Kelley, Electrochemical Methods for the Analysis of Clinically Relevant Biomolecules, Chem Rev 116 (2016) 9001–9090. https://doi.org/10.1021/acs.chemrev.6b00220.

[16] S.B. Prasanna, A.A.A. Bahajjaj, Y.H. Lee, Y.C. Lin, U. Dhawan, R. Sakthivel, R.J. Chung, Highly responsive and sensitive non-enzymatic electrochemical sensor for the detection of β-NADH in food, environmental and biological samples using AuNP on polydopamine/titanium carbide composite, Food Chem 426 (2023) 136609. https://doi.org/10.1016/j.foodchem.2023.

[17] A.F. Santidrian, A. Matsuno-Yagi, M. Ritland, B.B. Seo, S.E. LeBoeuf, L.J. Gay, T. Yagi, B. Felding-Habermann, Mitochondrial complex I activity and NAD+/NADH balance regulate breast cancer progression, Journal of Clinical Investigation 123 (2013) 1068–1081. https://doi.org/10.1172/JCI64264.

[18] M. Mohammadtaheri, R. Ramanathan, V. Bansal, Emerging applications of metal-TCNQ based organic semiconductor charge transfer complexes for catalysis, Catal Today 278 (2016) 319–329. https://doi.org/10.1016/j.cattod.2015.11.017.

[19] R. Precht, S. Stolz, E. Mankel, T. Mayer, W. Jaegermann, R. Hausbrand, Investigation of sodium insertion into tetracyanoquinodimethane (TCNQ): Results for a TCNQ thin film obtained by a surface science approach, Physical Chemistry Chemical Physics 18 (2016) 3056–3064. https://doi.org/10.1039/c5cp06659j.

[20] Y. Wei, X. Ren, H. Ma, X. Sun, Y. Zhang, X. Kuang, T. Yan, D. Wu, Q. Wei, In situ Formed Co(TCNQ)2 Metal-Organic Framework Array as a High-Efficiency Catalyst for Oxygen Evolution Reactions, Chemistry - A European Journal 24 (2018) 2075–2079. https://doi.org/10.1002/chem.201705606.

[21] M. Ballesteros-Rivas, A. Ota, E. Reinheimer, A. Prosvirin, J. Valdés-Martinez, K.R. Dunbar, Highly conducting coordination polymers based on infinite M(4,4′-bpy) chains flanked by regular stacks of non-integer TCNQ radicals, Angewandte Chemie - International Edition 50 (2011) 9703–9707. https://doi.org/10.1002/anie.201101658.

[22] R. Ramanathan, A.E. Kandjani, S. Walia, S. Balendhran, S.K. Bhargava, K. Kalantar-Zadeh, V. Bansal, 3-D nanorod arrays of metal-organic KTCNQ semiconductor on textiles for flexible organic electronics, RSC Adv 3 (2013) 17654–17658. https://doi.org/10.1039/c3ra43291b.

[23] R.A. Heintz, H. Zhao, X. Ouyang, G. Grandinetti, J. Cowen, K.R. Dunbar, New Insight into the nature of Cu(TCNQ): Solution routes to two distinct polymorphs and their relationship to crystalline films that display bistable switching behavior, Inorg Chem 38 (1999) 144–156. https://doi.org/10.1021/ic9812095.

[24] M. Mahajan, S.K. Bhargava, A.P. O'Mullane, Reusable surface confined semi-conducting metal-TCNQ and metal-TCNQF 4 catalysts for electron transfer reactions, RSC Adv 3 (2013) 4440–4446. https://doi.org/10.1039/c3ra22936j.

[25] M. Mahajan, S.K. Bhargava, A.P. O'Mullane, Electrochemical formation of porous copper 7,7,8,8-tetracyanoquinodimethane and copper 2,3,5,6-tetrafluoro-7,7,8,8-tetracyanoquinodimethane honeycomb surfaces with superhydrophobic properties, Electrochim Acta 101 (2013) 186–195. https://doi.org/10.1016/j.electacta.2012.09.068.

[26] S.A. O'Kane, R. Clérac, H. Zhao, X. Ouyang, J.R. Galán-Mascarós, R. Heintz, K.R. Dunbar, New crystalline polymers of Ag(TCNQ) and Ag(TCNQF4): Structures and magnetic properties, J Solid State Chem 152 (2000) 159–173. https://doi.org/10.1006/jssc.2000.8679.

[27] X. Mao, X. Wang, X. Xu, L. Jiang, J. Yang, Z. Du, Q. Kong, Preparation of reduced graphene oxide supported palladium nanocomposites for amperometric sensing of NADH, Int J Electrochem Sci 15 (2020) 6425–6435. https://doi.org/10.20964/2020.07.05.

[28] H. Kuhlenbeck, S. Shaikhutdinov, H.J. Freund, Well-ordered transition metal oxide layers in model catalysis - A series of case studies, Chem Rev 113 (2013) 3986–4034. https://doi.org/10.1021/cr300312n.

[29] Y. Ren, Z. Ma, P.G. Bruce, Ordered mesoporous metal oxides: Synthesis and applications, Chem Soc Rev 41 (2012) 4909–4927. https://doi.org/10.1039/c2cs35086f.

[30] G. Maduraiveeran, R. Ramaraj, Silver nanoparticles embedded in amine-functionalized silicate sol-gel network assembly for sensing cysteine, adenosine and NADH, Journal of Nanoparticle Research 13 (2011) 4267–4276. https://doi.org/10.1007/s11051-011-0372-5.

[31] G. Kianpour, F. Soofivand, M. Badiei, M. Salavati-Niasari, M. Hamadanian, Facile synthesis and characterization of nickel molybdate nanorods as an effective photocatalyst by co-precipitation method, Journal of Materials Science: Materials in Electronics 27 (2016) 10244–10251. https://doi.org/10.1007/s10854-016-5103-3.

[32] Y. Zhang, Y. Cai, J. Wang, L. Niu, S. Yang, X. Liu, Z. Zheng, L. Zeng, A. Liu, Cobalt-doped MoS2 nanocomposite with NADH oxidase mimetic activity and its application in colorimetric biosensing of NADH, Process Biochemistry 111 (2021) 178–185. https://doi.org/10.1016/j.procbio.2021.09.009.

[33] C.H. Chen, Y.C. Chen, M.S. Lin, Amperometric determination of NADH with Co3O4 nanosheet modified electrode, Biosens Bioelectron 42 (2013) 379–384. https://doi.org/10.1016/j.bios.2012.10.086.

[34] K.K. Maurya, K. Singh, M. Malviya, Effect of palladium and its nanogeometry on the redox electrochemistry of tetracyanoquinodimethane modified electrode; application in electrochemical sensing of ascorbic acid, J Appl Electrochem 53 (2023) 1–12. https://doi.org/10.1007/s10800-023-01878-z.

[35] Y. Li, W. Li, C. Yang, K. Tao, Q. Ma, L. Han, Engineering coordination polymer-derived one-dimensional porous S-doped Co3O4nanorods with rich oxygen vacancies as high-performance electrode materials for hybrid supercapacitors, Dalton Transactions 49 (2020) 10421–10430. https://doi.org/10.1039/d0dt02029j.

[36] Q. Lu, H. Wu, X. Zheng, Y. Chen, A.L. Rogach, X. Han, Y. Deng, W. Hu, Encapsulating Cobalt Nanoparticles in Interconnected N-Doped Hollow Carbon Nanofibers with Enriched Co-N-C Moiety for Enhanced Oxygen Electrocatalysis in Zn-Air Batteries, Advanced Science 8 (2021) 202101438. https://doi.org/10.1002/advs.

[37] G. Zhang, L. Liu, Q. Zhu, X. Kong, Chemoselective Hydrogenation of Nitroarenes by an Efficient Co@NC/AC Catalyst, Catal Letters 153 (2023) 1536–1542. https://doi.org/10.1007/s10562-022-04085-1.

[38] K. Singh, C. Singh, K.K. Maurya, M. Malviya, Redox electrochemistry of electrodes tuned with dimethyl ferrocene based on Co–NC–Pd nanogeometry: an impedimetric sensor for NADH sensing, Journal of Materials Science: Materials in Electronics 34 (2023) 1898. https://doi.org/10.1007/s10854-023-11257-1.

[39] S. Chen, L.L. Ling, S.F. Jiang, H. Jiang, Selective hydrogenation of nitroarenes under mild conditions by the optimization of active sites in a well defined Co@NC catalyst, Green Chemistry 22 (2020) 5730–5741. https://doi.org/10.1039/d0gc01835j.

[40] M. Li, C. Bao, Y. Liu, J. Meng, X. Liu, Y. Cai, D. Wuu, Y. Zong, T.P. Loh, Z. Wang, Reduced graphene oxide-supported cobalt oxide decorated N-doped graphitic carbon for efficient bifunctional oxygen electrocatalysis, RSC Adv 9 (2019) 16534–16540. https://doi.org/10.1039/c9ra02389e.

[41] S.E. Elugoke, O.E. Fayemi, A.S. Adekunle, P.S. Ganesh, S.Y. Kim, E.E. Ebenso, Sensitive and selective neurotransmitter epinephrine detection at a carbon quantum dots/copper oxide nanocomposite, Journal of Electroanalytical Chemistry 929 (2023) 117120. https://doi.org/10.1016/j.jelechem.2022.117120.

[42] P.S. Ganesh, A.B. Teradale, S.Y. Kim, H.U. Ko, E.E. Ebenso, Electrochemical sensing of anti-inflammatory drug mesalazine in pharmaceutical samples at polymerized-congo red modified carbon paste electrode, Chem Phys Lett 806 (2022) 140043. https://doi.org/10.1016/j.cplett.2022.140043.

[43] X. Wang, C. Hu, H. Liu, G. Du, X. He, Y. Xi, Synthesis of CuO nanostructures and their application for nonenzymatic glucose sensing, Sens Actuators B Chem 144 (2010) 220–225. https://doi.org/10.1016/j.snb.2009.09.067.

[44] J. Huang, Diffusion impedance of electroactive materials, electrolytic solutions and porous electrodes: Warburg impedance and beyond, Electrochim Acta 281 (2018) 170–188. https://doi.org/10.1016/j.electacta.2018.05.136.

[45] R. Vedalakshmi, V. Saraswathy, H.W. Song, N. Palaniswamy, Determination of diffusion coefficient of chloride in concrete using Warburg diffusion coefficient, Corros Sci 51 (2009) 1299–1307. https://doi.org/10.1016/j.corsci.2009.03.017.

[46] A.C. Lazanas, M.I. Prodromidis, Electrochemical Impedance Spectroscopy─A Tutorial, ACS Measurement Science Au 3 (2023) 162–193. https://doi.org/10.1021/acsmeasuresciau.2c00070.

[47] S. Immanuel, R. Sivasubramanian, Electrochemical kinetic investigation of NADH oxidation on Prussian blue-mediated chemically reduced graphene oxide nanosheets, Journal of Physics and Chemistry of Solids 161 (2022) 110471. https://doi.org/10.1016/j.jpcs.2021.110471.

[48] K. Guo, K. Qian, S. Zhang, J. Kong, C. Yu, B. Liu, Bio-electrocatalysis of NADH and ethanol based on graphene sheets modified electrodes, Talanta 85 (2011) 1174–1179. https://doi.org/10.1016/j.talanta.2011.05.038.

[49] C.H. Chen, Y.C. Chen, M.S. Lin, Amperometric determination of NADH with Co3O4 nanosheet modified electrode, Biosens Bioelectron 42 (2013) 379–384. https://doi.org/10.1016/j.bios.2012.10.086.

[50] S. Immanuel, R. Sivasubramanian, Electrochemical studies of NADH oxidation on chemically reduced graphene oxide nanosheets modified glassy carbon electrode, Mater Chem Phys 249 (2020) 123015. https://doi.org/10.1016/j.matchemphys.2020.123015.

[51] D. Gligor, Y. Dilgin, I.C. Popescu, L. Gorton, Poly-phenothiazine derivative-modified glassy carbon electrode for NADH electrocatalytic oxidation, Electrochim Acta 54 (2009) 3124–3128. https://doi.org/10.1016/j.electacta.2008.11.053.